NANO LETTERS

2008
Vol. 8, No. 2
411−414

Phase Diagram of Nanoscale Alloy Particles Used for Vapor–Liquid–Solid Growth of Semiconductor Nanowires

Eli Sutter* and Peter Sutter

Center for Functional Nanomaterials, Brookhaven National Laboratory, Upton, New York 11973

Received August 7, 2007; Revised Manuscript Received December 20, 2007

ABSTRACT

We use transmission electron microscopy observations to establish the parts of the phase diagram of nanometer sized Au–Ge alloy drops at the tips of Ge nanowires (NWs) that determine their temperature-dependent equilibrium composition and, hence, their exchange of semiconductor material with the NWs. We find that the phase diagram of the nanoscale drop deviates significantly from that of the bulk alloy, which explains discrepancies between actual growth results and predictions on the basis of the bulk-phase equilibria. Our findings provide the basis for tailoring vapor–liquid–solid growth to achieve complex one-dimensional materials geometries.

Semiconductor nanowires (NWs)—promising materials for quantum devices utilizing carrier confinement,[1] as well as photovoltaic cells[2] and sensors[3] taking advantage of a large surface-to-volume ratio—have been realized successfully by vapor−liquid−solid (VLS) growth. The VLS process was described for the first time in the 1960s for the formation of Si "whiskers"[4] and is now being used to synthesize NWs from a large variety of materials.[5] Yet, despite its widespread use, key aspects of the VLS growth process remain poorly understood, primarily due to the fact that, in contrast to studies on conventional thin film deposition, measurements with nanometer spatial resolution are needed to analyze the mechanisms of NW growth. Central to the VLS process is a liquid metal-semiconductor binary alloy drop whose interface to the semiconductor wire represents the NW growth front. Under steady-state growth conditions, adsorption on the drop maintains a concentration gradient of the semiconductor component of the liquid alloy, which is counteracted by a diffusion current through the drop. This liquid-phase transport, in turn, causes a small supersaturation driving the incorporation of new semiconductor material at the drop−NW interface to extend the wire.[6]

The properties of the alloy drop at or close to thermodynamic equilibrium with the adjacent NW, represented by the phase diagram of the binary alloy, govern important aspects of VLS NW growth. A key parameter is the equilibrium composition of the alloy, given by the liquidus line in the phase diagram. If the temperature of the alloy drop is changed, it spontaneously adjusts to a new equilibrium composition by exchange of semiconductor material with the adjacent solid NW, which leads to a well-defined adjustment of the drop size. The drop size, in turn, defines the diameter of the growing NW,[7] a key characteristic that governs, via quantum confinement, the electronic structure of the wire.[8] Although the one-to-one relationship between drop size and wire diameter has been recognized and used to tune the *overall* NW geometry, control over the *local*, position-dependent diameter, e.g., to induce constricted or dilated sections with a locally increased or decreased band gap along a NW, has not been demonstrated to date. A major step toward such new wire geometries, and toward increased control over VLS growth in general, lies in the determination of the phase diagram of the binary alloy drop for the relevant temperature range. Given the small drop size, typically few tens of nanometers, the phase diagram of the corresponding *bulk* alloy cannot be expected to accurately reflect the behavior of the VLS seed drop. Indeed, there are often discrepancies between actual growth results and predictions on the basis of the bulk phase diagram.[9]

Here we present real-time observations by high-resolution transmission electron microscopy (TEM) of Au−Ge alloy drops at the tips of Ge NWs, in the temperature range relevant for VLS growth of Ge wires (300−500 °C). *In situ* observations at the growth temperature are a powerful approach to quantifying equilibrium properties of the NW growth front, as well as the NW growth kinetics,[10] and can be used for exploring conditions suitable for the synthesis of complex NW geometries and heterostructures.[11,12] Our experiments show a pronounced, temperature-dependent exchange of Ge between the NW and the Au−Ge drop, in

* Author to whom correspondence should be addressed. Telephone: 631-344-7179. Fax: 631-344-3093. E-mail: esutter@bnl.gov.

10.1021/nl0719630 CCC: $40.75
Published on Web 01/15/2008

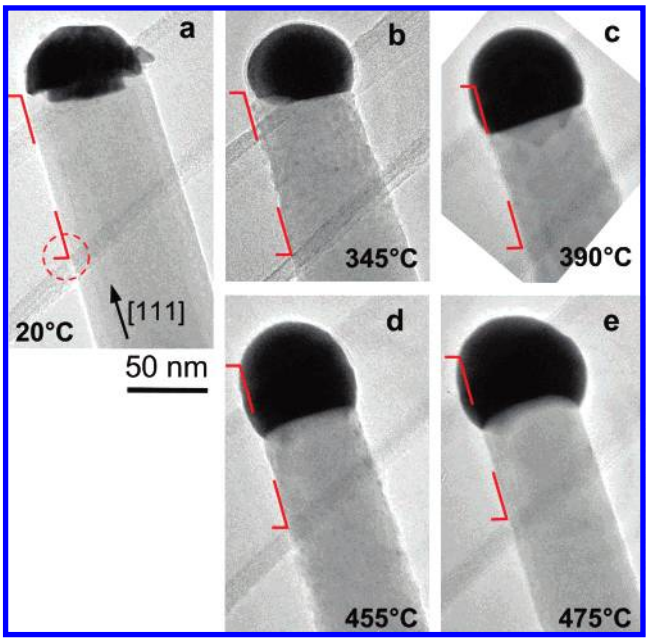

Figure 1. Sequence of TEM images showing a Ge NW adjacent to the Au−Ge alloy nanoparticle at the NW tip during *in situ* annealing at different temperatures between room temperature and 475 °C. (a) As-grown Ge NW at room-temperature prior to the annealing experiments; (b) Crystalline Au−Ge alloy nanoparticle before surface melting starts; (c−e) Exchange of material across the Ge NW/liquid drop interface after melting of the alloy Au−Ge nanoparticle at 368 °C. The marker delineate the surface of the Ge NW and provide a reference for the *T*-dependent location of the Au−Ge/Ge interface.

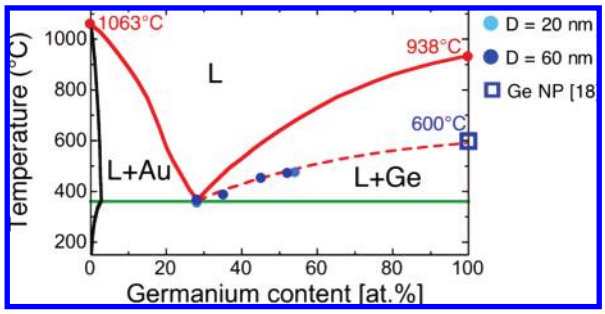

Figure 2. Au−Ge binary alloy phase diagram.[16] The solid red and green curves represent the Au and Ge liquidus and solidus lines, respectively. Dots represent measurements of the temperature-dependent Ge content of two Au−Ge alloy nanoparticles with radii of 10 and 30 nm at the tip of Ge NWs. The dashed red line is the bulk Ge liquidus line, scaled for best fit with the experimental data; the blue square represents the calculated melting temperature of a Ge nanoparticle with 26 nm diameter.[18] "L": liquid Au−Ge.

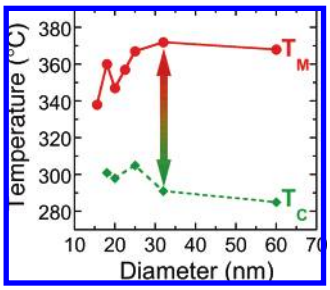

Figure 3. Dependence of the melting and crystallization temperature of Au−Ge nanoparticles at the tip of Ge NWs as a function of the NW diameter. The arrow indicates the supercooling for a NW with diameter of 32 nm.

which the wire acts as an efficient source or sink of Ge as the drop adjusts its composition to achieve its equilibrium Ge content. The *in situ* experiments, albeit not incorporating a growth flux and the small (∼2%)[13] supersaturation that drives actual NW growth, allow us to quantitatively determine important parts of the phase diagram of nanometer-sized Au−Ge VLS seed drops.

Variable temperature *in situ* experiments are carried out in a JEOL JEM 3000F field emission TEM equipped with a Gatan 652 high-temperature sample holder. They cover the temperature range between room temperature and 500 °C at pressures below 2×10^{-5} Pa. Electron irradiation intensity was kept below 2 A/cm^2 to prevent any uncontrolled electron beam induced structural changes. The Ge NWs were synthesized prior to the *in situ* studies by chemical vapor deposition from GeH_4 over a Au catalyst on a Si substrate at ∼320 °C in a UHV reactor with a base pressure of 2×10^{-10} Torr. They were then transferred through air and dispersed on amorphous carbon films supported by standard Cu grids for variable temperature TEM imaging.

Figure 1a shows a bright field TEM image of a typical Ge NW segment close to the tip, obtained at room-temperature prior to our *in situ* experiments. The electron beam was aligned with the [$\bar{2}$11] direction of the nanowire, so that fringes due to (111) lattice planes, perpendicular to the wire axis, were clearly resolved (see Supporting Information, Figure S-1). The slightly tapered NWs[14] have monocrystalline cores, are aligned with the [111] direction, and are initially terminated by a thin oxide layer formed during transfer in air. The Au-rich alloy nanoparticle at the tip is clearly distinguished by its darker contrast. Figure 1a−e follow the evolution of the nanoparticle and its interface with the wire during heating from room temperature to 475 °C. Initial heating to 300 °C, where the particle is still solid, causes the desorption of the native oxide from the Ge surface (Figure 1b).[14] Above 345 °C surface melting develops gradually, preceding the melting of the entire drop (see Supporting Information for observations of the melting process). The final melting of this nanoparticle—as the alloy achieves the (eutectic) composition with the lowest melting point by dissolving Ge from the NW—is observed at a eutectic temperature $T_E = 368$ °C. Our images show a large volume change upon melting as well as a simultaneous recession of the alloy−NW interface, as the alloy absorbs the Ge required to reach the eutectic composition. A further increase of the temperature to 475 °C $\gg T_E$ is accompanied by a continuous increase of the volume of the now liquid alloy drop (Figure 1e). Again, the interface between the alloy and the adjacent solid Ge NW draws back toward the base of the NW. Between room temperature and 475 °C the drop/NW interface draws back by ∼25−30 nm and transforms from a planar Ge (111) facet to a multifaceted interface composed of {113} and (111) segments. As a result, a substantial amount of Ge from the NW is incorporated in the alloy drop, increasing its volume and shifting its composition toward higher Ge concentration.

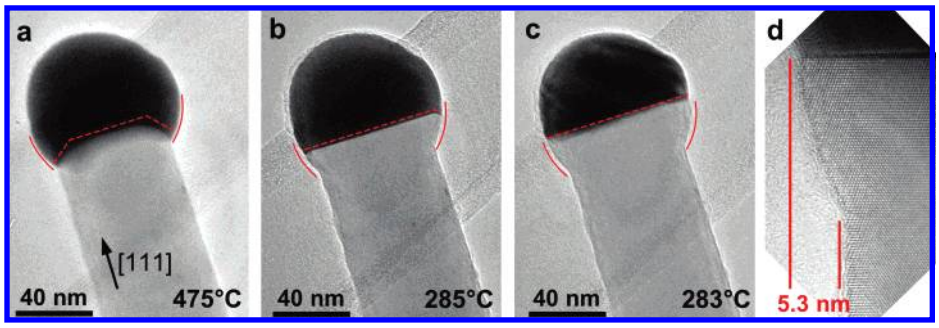

Figure 4. (a−c) Sequence of TEM images showing a liquid Au−Ge alloy drop at the tip of a Ge NW at different temperatures during cooling from 475 °C to solidification, which for this sample occurred at 283 °C. Note that the drop is still liquid at 285 °C. Curved red lines delineate the shape of the Au−Ge alloy drop at 475 °C. Dashed lines in indicate the projected shape of the interface between the Ge NW and the Au−Ge drop. (d) High-resolution TEM image of the expanded section of a Ge NW, after annealing to 475 °C and cooling to 280 °C.

We have used measurements of the drop volume to quantify the alloy composition as a function of temperature. The Ge content, N_{Ge}, was calculated from the volume of the eutectic drop, $V(T)$, using $N_{Ge} = (V(T) - N_{Au}\upsilon_{Au})/\upsilon_{Ge}$, where N_{Au} is the (constant) number of Au atoms in the drop and υ_{Au}, υ_{Ge} denote the atomic volumes of the alloy components, determined from the densities of liquid Au ($\rho_{Au} = 17.4 \times 10^3$ kg/m^3) and Ge ($\rho_{Ge} = 5.49 \times 10^3$ kg/m^3), respectively. We assume that the initial, solid particle at room temperature consists of pure Au (i.e., that all Ge is expelled by phase separation upon solidification). In situ energy dispersive X-ray spectrometry shows minimal amounts of Ge in the particle, evaluated to be less than 4 at. % (see Supporting Information, Figure S-2) in agreement with earlier observations of Ge content even below the detection limit in the Au seed particles.[15] With this assumption, we find a composition of the liquid drop at the melting temperature very close (within ±2 at. %) to the bulk eutectic composition (28 at. % Ge).[16]

In equilibrium, the Ge concentration of the alloy, $x(T) = N_{Ge}/(N_{Au} + N_{Ge})$, traces the liquidus of the *nanoscale* Au−Ge drop in VLS growth. Figure 2 compares the measured liquidus for NWs with diameters of 60 nm (shown in Figure 1) and 20 nm with the bulk phase diagram of the Au−Ge binary alloy. While the eutectic temperatures (T_E) are very close to $T_{E,\infty}$ of the bulk alloy, the nanometer-sized drops have substantially higher Ge content than a bulk Au−Ge alloy at temperatures $T > T_E$, i.e., the liquidus temperature is depressed and the Ge content and volume of the VLS seed drop much lower than predicted by the bulk phase diagram. The lowered liquidus tends toward a significantly reduced melting temperature for a pure Ge nanoparticle. Large melting point depressions are often observed for nanoparticles.[17] The size dependence of the melting temperature can be estimated using the well-established dependence $T_m = T_{m,\infty}[1 - \alpha/d]$, for spherical particles with diameter d, where $T_{m,\infty}$ denotes the bulk melting temperature and α depends on the surface to volume ratio and on the surface tensions of the liquid and solid.[18] For Ge, the predicted melting temperatures fall between 530 and 800 °C for particles with diameters between 20 and 60 nm. Extrapolating our experimental points for the Ge NW liquidus, using the functional form of the bulk liquidus,[16] to the melting temperature of a pure Ge nanoparticle gives $T_m \approx 600$ °C, equivalent to the predicted T_m of a nanoparticle with a 26 nm diameter, and in excellent agreement with the observed melting temperature of a NW with a 20 nm diameter.[19]

An immediate consequence of the liquidus suppression in the nanoscale Au−Ge phase diagram—important for VLS synthesis of Ge NWs—follows from the fact that the size of the alloy drop determines the wire diameter. While the bulk phase diagram predicts a negligible increase in drop size between T_E and 500 °C, the actual phase diagram implies a substantial size range in which the drop (and hence wire) diameter should be adjustable by judicious changes in temperature.

We have used further *in situ* observations at high temperature to demonstrate the controlled expansion of the NW diameter by tuning the size of the Au−Ge drop and to establish the microscopic mechanism by which this expansion occurs. In these experiments we use a large hysteresis between melting and crystallization temperatures (i.e., supercooling) of the alloy drops terminating our Au−Ge NWs, shown in Figure 3. The temperatures of melting and crystallization depend on the size of the Au−Ge particle. For very small diameters, the melting point is depressed by about 20 °C, while the observed crystallization temperature increases slightly, possibly indicating a surface induced crystallization process similar to that observed on free-standing Au−Ge drops.[20] The difference between melting and crystallization provides a temperature window below T_E in which a cooling drop remains liquid, i.e., traces the extension of the liquidus line for temperatures $T < T_E$. The supercooled drop maintains its equilibrium composition by expelling Ge, which becomes incorporated in the interfacial facets of the Ge NW. This behavior allows us to effectively probe the growth of a short NW section without driving the system out of equilibrium by an actual Ge flux onto the alloy drop. Annealing at $T_{max} \gg T_E$ (Figure 4) enlarges the Au−Ge drop by Ge absorption from the NW to a diameter of 75 nm, 20% larger that the original wire diameter (~60 nm). As the temperature is lowered the NW regrows, but with a new diameter ($d_{NW} \approx 75$ nm) defined by the now larger drop.

Two modifications of the Ge-rich alloy drop at high temperature are key to enabling the expansion of the Ge wire: a substantial growth of the drop volume, as seen from

the phase diagram, and an adjustment of the Au−Ge/Ge interface. The solid−liquid interface reshapes from a planar Ge (111) facet to a multifaceted interface, consisting of a central (111) plane surrounded by {113} facet segments at the periphery. The net result is a significantly larger footprint of the Au−Ge drop perpendicular to the wire axis, a prerequisite for the growth of a thicker NW, which is initiated by lowering the temperature (Figure 4a). As the cooling alloy drop reduces its Ge content by incorporation into the NW, the shape of the newly grown NW section closely follows the shape of the liquid alloy drop (Figure 4b,c). Experiments on etching and growth have shown that {113} is a fast growing facet for Ge,[21] while incorporation into the (111) plane is much slower. Hence, the initial wire growth from the cooling drop is accommodated almost entirely on the {113} facets, which supports the dilation of the NW diameter. Only when the {113} segments are completely outgrown is Ge incorporated into the (111) interface plane (Figure 4c). The material mediating the expansion of the NW diameter is perfectly crystalline Ge, without any observable defects (Figure 4d).

The expansion of the NW diameter critically depends on the annealing-induced swelling of the VLS alloy drop and on the reshaping of the solid−liquid interface. Control experiments, in which these effects were suppressed by limiting the maximum temperature to a few degrees above the melting point, i.e., $T_{max} \approx T_E$, resulted again in NW regrowth due to the melting-crystallization hysteresis, but with the original, smaller wire diameter.

Our in situ observations demonstrate that consideration of the actual phase diagram of a nanoscale VLS seed drop can be used to judiciously tailor the geometry of a growing NW. A junction where the NW diameter increases over a section of a few nanometers is achieved by a controlled expansion of the Au−Ge drop, following the liquidus of the nanodrop phase diagram. In practice, it will entail an interruption of the growth, annealing at a higher temperature to absorb additional semiconductor from the NW into the alloy drop, and finally a lowering of the temperature to expand to a new, larger wire diameter. Further VLS NW growth will maintain the larger diameter of the wire. Our observations show that even moderate annealing temperatures above the eutectic point provide a substantial potential for tailoring the NW geometry, while a negligible effect would be predicted by the bulk phase diagram. These findings clearly emphasize the need for quantitative, spatially resolved measurements to unleash the technological potential of semiconductor nanowires and related functional nanomaterials.

Acknowledgment. Work was performed under the auspices of the U.S. Department of Energy under Contract No. DE-AC02-98CH1-886.

Supporting Information Available: Additional information on melting of Au-Ge alloy nanoparticles. This material is available free of charge via the Internet at http://pubs.acs.org.

References

(1) Lu, W.; Xiang, J.; Timko, B. P.; Wu, Y.; Lieber, C. M. One-dimensional hole gas in germanium/silicon nanowire heterostructures. *Proc. Nat. Acad. Sci. U.S.A.* **2005**, *102*, 10046.
(2) Peng, K.; Xu, Y.; Wu, Y.; Yan, Y.; Lee, S.-T.; Zhu, J. Aligned single-crystalline Si nanowire arrays for photovoltaic applications. *Small* **2005**, *1*, 1062.
(3) Kamins, T. I.; Sharma, S.; Yasser, A. A.; Li, Z.; Straznicky, J. Metal-catalyzed, bridging nanowires as vapor sensors and concept for their use in sensor system. *Nanotechnology* **2006**, *17*, S291.
(4) Wagner, R. S.; Ellis, W. C. Vapor-liquid-solid mechanism of single crystal growth. *Appl. Phys. Lett*. **1964**, *4*, 89.
(5) Duan, X. F.; Lieber, C. M. General Synthesis of Compound Semiconductor Nanowires. *Adv. Mater*. **2000**, *4*, 298. Duan, X. F.; Huang, Y.; Cui, Y.; Wang, J. F.; and Lieber, C. M. InP Nanowires as building blocks for nanoscale electronic a d optoelectronic devices. *Nature* **2001**, *409*, 66. Kamins, T. I.; Li, X.; Williams, R. S. Growth and structure of chemically Vapor Deposited Ge Nanowires on Si Substrates. *Nano Lett*. **2004**, *4*, 503.
(6) Givargizov, E. I. Fundamental aspects of VLS growth. *J. Cryst. Growth* **1975**, *31*, 20.
(7) Cui, Y.; Lauhon, L. J.; Gudiksen, M. S.; Wang, J.; and Lieber, C. M. Diameter-controlled synthesis of single-crystal silicon nanowires. *Appl. Phys. Lett*. **2001**, *78*, 2214.
(8) Yang, J. E.; Chapter, B.; Jin, Chapter.; Kim, J.; and Jo, M. H. Band-Gap Modulation in Single Crystalline SiGe Nanowires. *Nano Lett*. **2006**, *6*, 2679; Delley, B.; and Steigmeier, E. F. Size Dependence of Band Gaps in Silicon Nanostructures. *Appl. Phys. Lett*. **1995**, *67*, 2370.
(9) Wu, Y.; Cui, Y.; Huynh, L.; Barrelet, C.; Bell , D.; and Lieber, C. Controlled growth and structures of molecular scale Si nanowires. *Nano Lett*. **2004**, *4*, 433. Wu, Y.; Yang, P. Direct observation of the vapor-liquid-solid nanowire growth. *J. Am. Chem. Soc*. **2001**, *123*, 3165.
(10) Kodambaka, S.; Tersoff, J.; Reuter, M. C.; Ross, F. M. Ge Nanowire Growth Below the Eutectic Temperature. *Science* **2007**, *316*, 729.
(11) Lauhon, L. J.; Gudiksen, M. S.; Lieber, C. M. Semiconductor Nanowire Heterostructures. *Phil. Trans. R. Soc. London, Ser. A* **2004**, *362*, 1247. Lauhon, L. J.; Gudiksen, M. S.; Wang, D.; Lieber, C. M. Epitaxial Core-Shell and Core-Multishell Nanowire Heterostructures. *Nature* **2002**, *420*, 57. Wu, Y.; Xiang, J.; Yang, C.; Lu, W.; Lieber, C. M. Single-crystal metallic nanowires and metal/semiconductor nanowire heterostructures. *Nature* **2004**, *430*, 61.
(12) Sköld, N.; Karlsson, L. S.; Larsson, M. W.; Pistol, M.-E.; Seifert, W.; Traghardh, J.; Samuelson, L. Growth and optical properties of strained GaAs-GaInP core-shell nanowires. *Nano Lett*. **2005**, *5*, 1943.
(13) Tromp, R. M.; Mankos, M. Thermal Adataoms on Si. *Phys. Rev. Lett*. **1998**, *81*, 1050.
(14) Sutter, E.; Sutter, P. Au-induced encapsulation of Ge nanowires in protective carbon shells. *Adv. Mater*. **2006**, *18*, 2583.
(15) Sun, X. H.; Didychuk, C.; Sham, T. K.; Wong, N. B. Ge Nanowires: Synthesis, morphology and local structural studies. *Nanotechnology* **2006**, *17*, 2925.
(16) Predel, B. Phase Equilibria. In *Crystallographic and Thermodynamic Data of Binary Alloys − Electronic Materials and Semiconductors, Landolt-Bornstein, Group IV: Physical Chemistry, Vol. 5*; Madelung, O., Ed.; Springer: Berlin, 1998.
(17) For instance, see: Goldstein, A. N.; Ecker, C. M.; Alivisatos, A. P. Melting in Semiconductor Nanocrystals. *Science* **1992**, *256*, 1425. Chiu, H. W.; Kauzlarich, S. M.; Sutter, E. Thermal Behavior and Film Formation from an Organogermanium Polymer Nanoparticle Precursor. *Langmuir* **2006**, *22*, 5455.
(18) Wautelet, M. Estimation of the variation of the melting temperature with th esize of small particles, on the basis of the surface-phonon instability. *J. Phys. D Appl. Phys.* **1991**, *24*, 343.
(19) Wu, Y.; Yang, P. Melting and welding of semiconductor nanowires in nanotubes. *Adv. Mater*. **2001**, *13*, 520.
(20) Sutter, P.; Sutter, E. Dispensing and surface-induced crystallization of zeptoliter liquid metal-alloy drops. *Nat. Mater*. **2007**, *6*, 363.
(21) Vescan, L.; Grimm, T.; Dieker, K. Facet investigation of selective epitaxial growth of Si and SiGe on (001) Si for optoelectronic devices. *J. Vac. Sci Technol*. **1998**, *16*, 1549. Arizumi and Akasaki, I. Etch patterns and dislocation etch pits on germanium with KI-I2 redox system. *Jpn. J. Appl. Phys*. **1962**, *1*, 350.

NL0719630